

Analysis of the blowout plasma wakefields produced by drive beams with elliptical symmetry

P. Manwani,* Y. Kang, J. Mann, B. Naranjo, G. Andonian, and J. B. Rosenzweig
Department of Physics and Astronomy, UCLA, Los Angeles, California 90095, USA

(Dated: November 21, 2024)

In the underdense or blowout regime of plasma wakefield acceleration, the particle beam is denser than the plasma. Under these conditions, the plasma electrons are nearly completely rarefied from the beam channel, resulting in a nominally uniform ion column. Extensive investigations of this interaction assuming axisymmetry have been undertaken. However, the blowout produced by a transversely asymmetric driver, which would be present in linear collider "afterburner" scenarios, possesses quite different characteristics. Such beams create an asymmetric plasma rarefaction region which leads to asymmetric focusing in the two transverse planes, accompanied by a non-uniform accelerating gradient. The asymmetric blowout cross-section is found through simulation to be elliptical, and treating it as such permits simple extension of the symmetric theory. In particular, focusing fields which are linear in both transverse directions exist in the bubble. The form of the wake potential and the associated beam matching conditions in this elliptical cavity are discussed. We also discuss blowout boundary estimation in the long driver limit and applications of the salient asymmetric features of the wakefield.

Plasma wakefield acceleration (PWFA) is an emerging technique for high energy accelerator applications such as particle colliders and free-electron lasers. In PWFA, electromagnetic fields in excess of 1000 times that of conventional technology are attainable, enabling compact and efficient acceleration of charged particles at the highest energies. Of particular interest is application to next generation particle colliders, which require high luminosity at interaction. Collider designs for high luminosity rely on the generation and transport of beams with high-aspect ratio transverse asymmetry, with associated large ratio of the normalized emittances employed in the transverse planes. This approach minimizes strong beam-beam forces and radiative energy spread (beamstrahlung) [1] at the interaction point. These asymmetric (flat) beams are proposed for use in "plasma afterburners", which seek to extend the energy reach of an existing linear collider based on standard techniques [2]. While detailed PWFA-collider conceptual designs have been proposed, the study of flat beam based PWFAs is not yet developed. Thus, the plasma response and associated dynamics and evolution of flat beam properties, which are the themes of this Letter, is ripe for analytical and experimental investigation.

While the PWFA was initially proposed in the linear [3] regime, where it is based on simple plasma electron oscillations harmonic at the plasma frequency $\omega_p = \sqrt{e^2 n_0 / \epsilon_0 m_e}$, where n_0 is the nominal plasma density, it is now most commonly used in the nonlinear (blowout) [4, 5]. In the blowout case, where the beam density n_b greatly exceeds n_0 , the strong electric fields of the driver expel the plasma electrons outward, creating a blowout cavity (or bubble) entirely devoid of electrons. The expelled electrons and the electrons within a plasma skin-depth, $k_p^{-1} = c/\omega_p$, boundary form a dense electron sheath which envelops the cavity. This high local plasma

electron density region and the associated return current shield the drive beam's electromagnetic (EM) fields outside of the bubble region [4, 6, 7]. The forces acting on the beam inside of this axisymmetric bubble are quite ideal for high quality acceleration, with no dependence of longitudinal forces on transverse offset. Further, due to the uniform ion column inside the bubble, the electrons undergo linear, aberration-free focusing dependent only on radial offset.

While axisymmetric driver scenarios have been extensively studied (see also, *e.g.* [8] and [9]), there are still many open questions concerning the physics of plasma structures formed by strongly asymmetric drivers [10]. To start, one notes from in simulations that the blowout created by flat beams can be well-approximated to be elliptical in cross-section. Consequently, the potential inside these elliptical cavities, which are translating at nearly the speed of light (beam velocity $v_b \simeq c$), depends quadratically on transverse coordinates, yielding linear transverse electric fields that are different in the two transverse planes [11, 12]. This asymmetry in the transverse focusing fields provides unique focal properties, enabling the beam to be tightly focused in one plane. This may prove a key advantage in using plasma lenses as a final focusing system for next-generation colliders [13]. To proceed with the analysis of flat-beam scenarios, we use the three-dimensional particle-in-cell (PIC) code OSIRIS [14] to investigate the EM fields inside the elliptical blowout cavity. We then employ these phenomenological results to guide development of a theoretical model.

Throughout the remainder of this Letter we use normalized units, where densities are normalized to n_0 , which specifies the electron plasma frequency ω_p . With this fundamental scale specified, a unitless notation is implemented as follows: time is normalized to ω_p^{-1} ; velocities to the speed of light c ; masses to the electron

mass m_e ; distance to the plasma skin-depth $k_p^{-1} = c/\omega_p$; charge to e ; and EM field amplitudes to the so-termed wave-breaking [15] value, $E_{WB} m_e c \omega_p / e$. The source terms in our model and their species is indicated using the following subscripts: the plasma ions (i), the plasma electrons (e), and the drive beam (b).

To simplify our analysis, we make the common assumption that the massive ions are static, forming a uniform background charge of $n_i = 1$. This assumption holds when the oscillation phase advance of the ions in the potential of the beam is small, $\Delta\phi = \sigma_z \sqrt{\pi Z_i n_b / m_i} \ll 1$, where Z_i is the ionization state of the ions, m_i is the ion mass, and σ_z is the beam bunch length [16]. The EM source terms are then given by: the charge density $\rho = \rho_b + \rho_e + 1$ and the current density $\mathbf{J} = \mathbf{J}_b + \mathbf{J}_e$.

The equations of motion for the plasma electrons can be written in Hamiltonian form by using the vector and scalar potentials \mathbf{A} , respectively, and ϕ , and the canonical momenta $\mathbf{P} = \mathbf{p} + \mathbf{A}$. The beam evolution occurs on a much larger time-scale than the plasma wakefield in the co-moving frame, thus permitting use of the quasi-static approximation $(x, y, z, t) \rightarrow (x, y, \xi \equiv t - z, s \equiv z)$ [17], where we describe a slowly-varying disturbance in s , quantified through derivatives by $\partial_s \ll \partial_\xi$.

With this approximation, Maxwell's equations for the normalized potentials in the Lorentz gauge reduce to

$$\nabla_\perp^2 \begin{bmatrix} \phi \\ \mathbf{A} \end{bmatrix} = - \begin{bmatrix} \rho \\ \mathbf{J} \end{bmatrix}, \quad (1)$$

where $\nabla_\perp^2 = \partial_x^2 + \partial_y^2$ is the transverse Laplace operator. The Lorentz gauge condition $\nabla \cdot \mathbf{A} + \frac{\partial \phi}{\partial t} = 0$ can now be written as $\nabla_\perp \cdot \mathbf{A}_\perp = -\frac{\partial}{\partial \xi}(\phi - A_z) = -\frac{\partial}{\partial \xi}\psi$. Here $\psi = \phi - A_z$ is the wake potential, which obeys the transverse Poisson equation $-\nabla_\perp^2 \psi = \rho - J_z = S$. Here we have defined a new effective source density S . The continuity equation in the ξ -frame can be written as $\frac{\partial}{\partial \xi} S + \nabla_\perp \cdot \mathbf{J}_\perp = 0$. Now, the Hamiltonian is given by $\bar{H} = \gamma - \phi$ with the Lorentz factor $\gamma = \sqrt{1 + |\mathbf{p}|^2}$. In the quasi-static approximation, the Hamiltonian depends on z and t only through $\xi = t - z$. Hamilton's equations give $\frac{dH}{dt} = \frac{\partial H}{\partial t} = \frac{\partial H}{\partial \xi} = -\frac{\partial H}{\partial z} = \frac{dP_z}{dt}$, yielding conservation of $\bar{H} - P_z$. If the electrons are initially at rest, this implies, $\gamma - \phi - p_z + A_z = 1$ [18, 19]. After substituting for the wake potential, this initial condition gives

$$\gamma - \psi - p_z = 1. \quad (2)$$

The E_i fields are found from the potentials as follows:

$$\begin{aligned} E_z &= \frac{\partial \psi}{\partial \xi}; \quad \mathbf{E}_\perp = -\nabla_\perp \phi - \frac{\partial \mathbf{A}_\perp}{\partial \xi}; \\ \mathbf{B}_\perp &= \nabla_\perp \times \mathbf{A}_z + \nabla_z \times \mathbf{A}_\perp; \quad B_z = \nabla_\perp \times \mathbf{A}_\perp \end{aligned} \quad (3)$$

Note that the forces on the beam in the ultra-relativistic limit $v_b = c$ they are all simply derived from ψ . Here we concentrate on the plasma response instead of the beam,

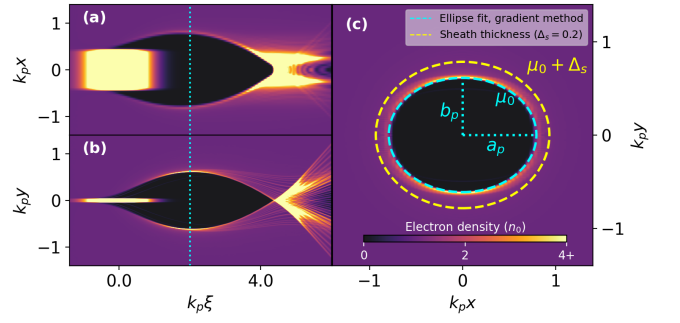


FIG. 1: Plasma wakefield created by a uniform current driver pulse with beam density $n_b = 15$, having spot sizes: $a = 0.424$, $b = 0.0424$. Longitudinal slices are shown in (a) the x - z plane and (b) the $-z$ plane, as well as the transverse slice displaying the elliptical profile.

and so the analysis of interest is more complex. Indeed, when the driver interacts with an underdense plasma, plasma electrons are strongly repelled by the first-order Coulomb force due to the beam charge, with magnetic effects becoming important for a relativistic plasma response, as is found in the blowout regime. This repulsion leads to strong, non-laminar plasma motion, which upon evacuation of the plasma electrons from the beam channel ultimately leads to the formation of a blowout sheath surrounding a plasma-electron-free cavity.

To obtain a preliminary understanding of this system in the case of an asymmetric drive beam, we first consult the results of EM PIC simulations (see Figure 1, which shows the output from the code OSIRIS [14]). In order to display the most general plasma response, we examine here a short-beam case, corresponding to excitation of large longitudinal wakes, and the dynamic evolution of the bubble dimensions. We will see that this scenario can be explained well by use of our theoretical model; further progress in understanding the interplay between plasma response and beam dynamics, we will subsequently concentrate on a long-beam analysis. This will permit useful results such as beam focal-matching conditions.

When considering an elliptically-shaped drive beam, the cross-sections of the blowout cavity and its accompanying boundary sheath also take elliptical shapes. The asymmetry of the wakefield produced by the elliptically-shaped beam are shown in the longitudinal slices displayed in Figure 1. The asymmetry drives sheath electron trajectories behind the blowout in a more complex manner than in the symmetric case, where the crossing of trajectories results in a large near-axis density spike; here this feature is missing. The transverse slice of the wakefield itself shows the elliptical cross-section created by the evacuated plasma electrons, measured by semi-axes a_p and b_p and accompanied by a thin, dense plasma electron sheath of width Δ_ρ . There is also a longitudinal plasma return current outside the bubble having thick-

ness k_p^{-1} , *i.e.* $\Delta_j \approx 1$. For the ease of analysis, we treat a full source sheath thickness, Δ_s , taken to be the same as the density sheath thickness, Δ_ρ , as $\rho - J_z \approx \rho$ [7]. For simplicity we take the sheath density distribution to be uniform and confocal with the ion column ellipse.

The confocal condition stems from our choice of a uniform beam distribution that does not vary with the angular coordinate, which was made due to its simplicity and alignment with observations. However, the confocal condition can be extended to other distributions that more closely match the spatial form of the sheath layer observed in simulations. We show in the Appendix that use of the confocal condition allows construction of a solution for the wake potential that vanishes outside the sheath, which is a direct consequence of the assumption that no EM fields exist outside the electron sheath.

We can integrate the charge continuity relation over the transverse plane, and with the divergence theorem we attain the conservation of the sources in each transverse plane, $\frac{d}{d\xi} \int S dA = 0$. With the absence of any source ahead of the driver, this conservation results in net zero source on each transverse plane, $\int S dA = 0$, permitting the sheath density to be found.

We now introduce elliptical coordinates (μ, ν) using the substitution $x = c_p \cosh \mu \cos \nu$ and $y = c_p \cosh \mu \sin \nu$, with μ_0 and $c_p = \sqrt{a_p^2 - b_p^2}$ defining the elliptical blowout boundary and focal length of the ellipse, respectively. The sheath is confocal to the ellipse defined by μ_0 . We can now construct the Poisson equation with the defined source terms for each transverse slice:

$$-\nabla_\perp^2 \psi = -\frac{2}{c_p^2 (\cosh 2\mu - \cos 2\nu)} \left(\frac{\partial^2 \psi}{\partial \mu^2} + \frac{\partial^2 \psi}{\partial \nu^2} \right) = \begin{cases} 1 & \mu < \mu_0, \\ -\frac{\sinh 2\mu_0}{\sinh(2\mu_0 + 2\Delta_s) - \sinh 2\mu_0} & \mu_0 < \mu < \mu_0 + \Delta_s, \\ 0 & \mu > \mu_0 + \Delta_s. \end{cases} \quad (4)$$

Here, we assume that Δ_s is small compared to μ_0 . We are interested in the solution of ψ inside the ellipse, and so we can expand the equation up to first order in Δ_s :

$$\psi|_{\mu < \mu_0} = -\frac{c_p^2}{8} \left[\cosh 2\mu - \cosh 2\mu_0 + \left(1 - \frac{\cosh 2\mu}{\cosh 2\mu_0} \right) \cos 2\nu \right] + \Delta_s \left(\sinh 2\mu_0 - \tanh 2\mu_0 \frac{\cosh 2\mu}{\cosh 2\mu_0} \cos 2\nu \right) \quad (5)$$

Converting the results to Cartesian coordinates using $x = c \cosh \mu \cos \nu$ and $y = c \sinh \mu \sin \nu$, we find

$$\psi(x, y) = -\frac{x^2 b_p^2 + y^2 a_p^2 - p_p^4}{2d_p^2} - \frac{\Delta_s p_p^2}{2d_p^4} \left[(x^2 - y^2) c_p^2 - a_p^4 - b_p^4 \right], \quad (6)$$

where $p_p^2 = a_p b_p$ and $d_p^2 = a_p^2 + b_p^2$. We note that this wake potential, which determines the motion of beam electrons within the blowout cavity, is quadratic in both x and y . As this potential is that of a two-dimensional simple-harmonic oscillator, focal characteristics and therefore matched (equilibrium propagation) beam conditions in both transverse planes can be derived from Eq. 6.

In general, the wakefields can be derived from the gradient of the wake potential, as:

$$\begin{aligned} W_x &= E_x - B_y = -\frac{\partial \psi}{\partial x} = x \left[\frac{b_p^2}{d_p^2} + \Delta_s \frac{p_p^2 c_p^2}{d_p^4} \right] \\ W_y &= E_y + B_x = -\frac{\partial \psi}{\partial y} = y \left[\frac{a_p^2}{d_p^2} - \Delta_s \frac{p_p^2 c_p^2}{d_p^4} \right] \\ W_z &= E_{z,p} = \frac{\partial \psi}{\partial \xi} = \frac{p^2}{d^4} \left[C_1 (x^2 - y^2) + C_2 \right] \\ &\quad + \frac{\Delta \mu}{2d^6} \left[C_3 (x^2 - y^2) + C_4 \right] \end{aligned} \quad (7)$$

where $'$ indicates the derivative with respect to ξ , $C_1 = a_p' b_p - b_p' a_p$, $C_2 = a_p' b_p^3 + b_p' a_p^3$, $C_3 = C_1 (a_p^4 - 6a_p^2 b_p^2 + b_p^4)$, and $C_4 = (a_p^6 + b_p^6)(p_p^2)' + (a_p^5)' b_p^3 - a_p^5 (b_p^3)' + a_p^3 (b_p^5)' - (a_p^3)' b_p^5$. We can estimate the physical size of the sheath thickness in the two transverse planes by reverting to Cartesian coordinates, *i.e.* $\Delta_x \approx b_p \Delta_s$ and $\Delta_y \approx a_p \Delta_s$. Note the linearity of W_x and W_y in x and y , respectively.

Simulations indicate that a thin sheath, $\Delta_s \lesssim 0.2$, yields reasonable results for W_x and W_y , so the electron sheath can be further approximated as infinitesimally thin, $\Delta_s \rightarrow 0$. We may then proceed without using the external fitting parameter adopted in Ref. [20]. Additionally, as we assume that no EM fields exist outside the cavity due to the shielding provided by the boundary sheath at the edge of the blowout area. We then can set ψ to be zero everywhere outside the blowout region, allowing us to write: $\nabla_\perp^2 \psi(\xi) = -1$, with $\psi|_{\partial\Omega(\xi)} = 0$, providing the same result as above without the sheath thickness parameter: $\psi = -(x^2 b_p^2 + y^2 a_p^2 - p_p^4)/2d_p^2$. In the axisymmetric limit $a_p = b_p$, and we attain the standard result $\psi_r = -(r^2 - r_b^2)/4$, where r is the radial coordinate and r_b is the blowout radius.

As anticipated, we validate our approach to the general flat beam PWFA by comparing the output of the PIC simulations with these analytical results. The axes of the resulting ellipse are found by numerically evaluating the boundary positions via a least-squares fitting of boundary points marking the position maximum gradient of density for 100 radial line searches taken at uniformly spaced angles. The relative root mean square error (RRMSE) between the PIC-simulated transverse fields and the fields predicted by Eq. 7 (with geometry found by the elliptical fit to the boundary points) is shown in Figure 2. The RRMSE is calculated by considering each data point within the blowout boundary,

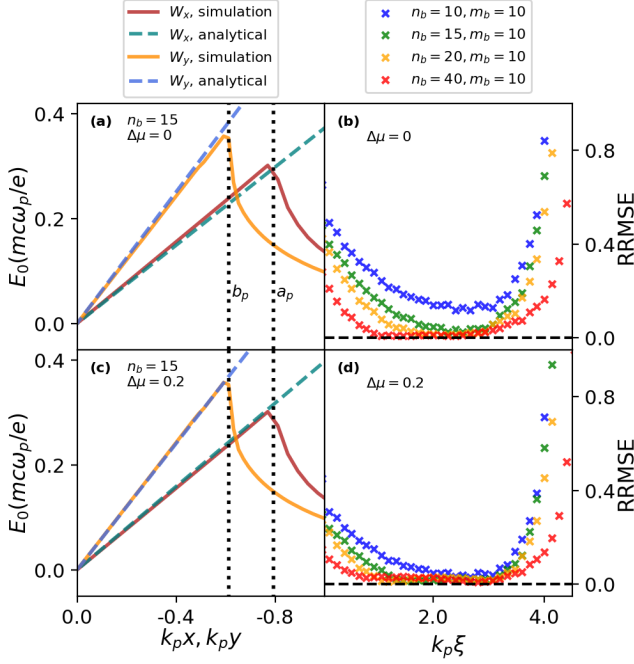


FIG. 2: Short beam ($\sigma_z = 0.5$) driver, corresponding to the case of Fig. 1. (a) Transverse wakefield line-outs of the wake. (b) Comparison between the analytical transverse wakefield W_\perp from different n_b , calculated using the fitted blowout boundary.

$\text{RRMSE} = \sqrt{\frac{1}{n} \sum_{i=1}^n (X_i - \hat{X}_i)^2} / (\frac{1}{n} \sum_{i=1}^n \hat{X}_i)$, with X_i representing the analytical fields and \hat{X}_i representing the PIC-simulated fields. The elliptical model's predictions for transverse wakes closely match simulations.

While this is not a main thrust of the current work, we add some relevant comments on the longitudinal wake W_z here. The Panofsky-Wenzel theorem [21] as applied to plasma wakefields gives $\nabla_\perp W_z = \partial_\xi W_\perp$. This follows from their description in terms of the potential ψ . In a symmetric blowout, W_z has been long known to be independent of x and y as a result of the constant nature of W_\perp after blowout, and is independent of the sheath thickness due to the wakefield axisymmetry. However, with an elliptical bubble shape, W_z becomes coordinate dependent and varies with the sheath thickness, due to dependencies on the shape of the ρ and J_z distributions.

To further extend the utility of our analytical results, we proceed to estimate the location of the elliptical boundaries using the beam parameters in the long beam limit, $k_p \sigma_z \gg 1$, neglecting the longitudinal variation of the fields in the beam region. We are searching for an equilibrium scenario, and we thus examine the force on the plasma electrons at a position \mathbf{r} near the sheath. Considering the plasma electron's transverse velocity $\mathbf{v}_\perp = d\mathbf{r}_\perp/dt = (1 - v_z) d\mathbf{r}_\perp/d\xi = \gamma^{-1}(1 + \psi) d\mathbf{r}_\perp/d\xi$

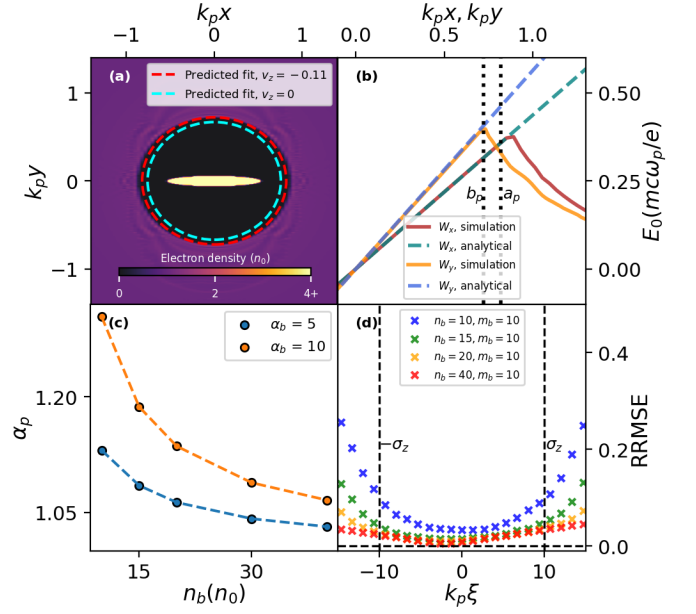


FIG. 3: Long beam ($\sigma_z = 10$) driver: (a) Analytical calculation for the blowout shape using a beam with $n_b = 20$, $a = 0.5$ and $b = 0.05$. (b) Transverse wakefield lineouts of the wake, calculated using the predicted blowout boundary. (c) predicted blowout ellipticity at the center of wake vs beam density and beam ellipticity. (d) Comparison between the analytically calculated transverse wakefield and the simulation results.

in combination with Eq. 2,

$$\mathbf{F}_\perp = (1 - v_z) \frac{d\mathbf{p}_\perp}{d\xi} = \frac{1}{\gamma} (1 + \psi) \frac{d}{d\xi} \left((1 + \psi) \frac{d}{d\xi} \mathbf{r}_\perp \right) \quad (8)$$

$$\mathbf{F}_\perp|_{\partial\Omega} = \frac{1}{\gamma} \left(\frac{d\psi}{d\xi} \frac{d\mathbf{r}_\perp}{d\xi} + \frac{d^2\mathbf{r}_\perp}{d\xi^2} \right) \Big|_{\partial\Omega} = 0, \quad (9)$$

where $\partial\Omega$ indicates the condition at the boundary sheath. Neglecting possible variations along ξ then allows us to balance the transverse forces at the boundaries. We also assume that the plasma electron longitudinal velocity v_z does not depend on the transverse coordinate. This facilitates the solution to the above equations by providing a linear relationship between ϕ_e and A_e , to which we can add v_z effects as a correction. Using Eq. 3 to convert to a potential description and assuming $v_b = 1$, we have

$$\mathbf{F}_\perp = \nabla_\perp \phi_i + \nabla_\perp \phi_e + \nabla_\perp \phi_b + \partial_\xi \mathbf{A}_\perp - (\nabla_\perp \mathbf{A}) \cdot \mathbf{v} - (\mathbf{v} \cdot \nabla) \mathbf{A}_\perp \quad (10)$$

With Eq. 9 and neglecting the longitudinal variation of the transverse velocity and fields leads to the relation

$$(1 + v_z) \nabla_\perp \psi|_{\partial\Omega} - v_z \nabla_\perp \phi_i|_{\partial\Omega} + (1 - v_z) \nabla_\perp \phi_b|_{\partial\Omega} = 0. \quad (11)$$

Since the cavity is effectively evacuated of plasma electrons, we can obtain the scalar potential due to the ions alone, $\phi_i(\xi) = -\frac{x^2 b_p(\xi) + y^2 a_p(\xi)}{2(a_p(\xi) + b_p(\xi))}$ [22]. We first neglect v_z to find the zero-th order equation in the electrostatic limit. Using Ampere's law, $\oint \mathbf{B} \cdot d\mathbf{l} = \int (\mathbf{J} + \epsilon_0 \frac{\partial \mathbf{E}}{\partial t}) \cdot d\mathbf{a}$, we integrate over the transverse plane to remove the left hand side term, finding $I_{z,beam} + I_{z,elec} + \int_0^\infty \frac{\partial^2 \psi}{\partial \xi^2} da = 0$. In the long beam limit, the integral term is neglectable. Consequently, this verifies the equivalence between the beam current and a plasma return current layer of thickness $\Delta_j = 1$. By assuming the v_z to be constant across this region, we find that $v_z = \frac{\lambda_b}{\pi(a_p+1)(b_p+1)}$, where λ_b is the beam charge per unit length. This enables us to incorporate the EM features of the sheath, beyond the zero-th order analysis above for weak blowout scenarios. For strong blowouts, a detailed treatment of the sheath is in principle important. Fortunately, in this limit an axisymmetric bubble shape is inherently approached and the details of the sheath fade in importance.

We thus use the electric fields of the elliptical drive beam [23] to simultaneously find ψ and the elliptical semi-axes a_p and b_p such that the transverse forces on the ellipse boundaries are minimized. Here $\alpha_p = a_p/b_p$ represents the ellipticity of the cavity. We verify our results by calculating the blowout shape for a long beam driver, predicting the transverse fields and calculating the RRMSE values in Fig. 3 (see Supplemental Material for the details on PIC simulations [24]). In this way, we demonstrate the capability of determining a_p and b_p .

We therefore have a path to determining self-consistently the beam sizes and blowout dimensions. The beam size is dependent on the emittance and the focusing strength of the linear field restoring forces on the beam. We write equations of motion for the transverse beam dynamics inside the asymmetric blowout cavity:

$$x''(z) + K_x x(z) = 0; \quad y''(z) + K_y y(z) = 0 \quad (12)$$

$$K_x = K_r \frac{2}{1 + \alpha_p^2}; \quad K_y = K_r \frac{2\alpha_p^2}{1 + \alpha_p^2} \quad (13)$$

where $K_r = 1/2\gamma$ arises from the normalized linear focusing strength of the ions in an axisymmetric ion column. It can be seen that the focusing is a superposition of monopole and quadrupole strengths (K_r and $K_r \frac{\alpha_p^2 - 1}{\alpha_p^2 + 1}$), respectively. This could be deduced directly from the elliptical symmetry of the charge distribution. The equilibrium propagation or *matching* conditions for a beam in the asymmetric bubble are then given by:

$$\sigma_{m,\eta} = \sqrt{\frac{\sqrt{K_\eta^{-1} \epsilon_{n,\eta}}}{\gamma}} \rightarrow \frac{\sigma_{m,x}}{\sigma_{m,y}} = \sqrt{\frac{\epsilon_{n,x}}{\epsilon_{n,y}} \alpha_p} \quad (14)$$

where $\eta \in \{x, y\}$ and $\epsilon_{n,\eta}$ are the normalized emittances. The the matched beam aspect ratio is determined by the combination of the emittance ratio and the ellipticity of the wake. This condition can be used to match the beam inside a given plasma profile through a simple iterative procedure we will describe in a subsequent paper.

Qualitatively, it can be seen that for strong blowouts where $\alpha_p \simeq 1$, the beams equilibrium sizes can be easily deduced from the well-known axisymmetric ion-column focusing conditions. In the weak blowout limit, the bubble boundary closely follows the beam contours ($\alpha_p \simeq \sigma_{m,x}/\sigma_{m,y}$), and one may deduce that $\sigma_{m,x}/\sigma_{m,y} \simeq \epsilon_{n,x}/\epsilon_{n,y}$. In weak blowout, the beam asymmetry is greatly increased by the associated focal asymmetry.

In this paper, we have created a phenomenological model for understanding the plasma structures formed by elliptical beams wake. We have concentrated on the crucial issue of the focusing forces in this scenario, which provoke significant changes in the beam dynamics significantly. These insights are essential for present plasma wakefield experiments and future plans for plasma afterburner colliders using asymmetric beams. The findings presented here shed light on the ellipticity and emittance requirements for achieving beam matching within the elliptical blowout cavity [25]. This approach can also be utilized in the context of laser wakefield acceleration (LWFA) [26], but care must be taken to treat the driver interactions due to the local nature of the ponderomotive force as compared with the long-range Coulomb interaction. The disparity in focusing forces in the two transverse planes presents unique challenges and opportunities. These include an experiment developed for the Argonne Wakefield Accelerator for examining the propagation of a particle beam in a plasma with asymmetric transverse emittances [27–29], as well as the development of an asymmetric plasma lens [30].

While this current Letter lays the foundation for understanding main points of a asymmetric wakefields driven by elliptically-shaped beams, further research is necessary to give as rich of an understanding as has been obtained axisymmetric beams in [6, 20]. Efforts aim to hone the tools introduced here are underway, as exemplified by the additional results given in the Supplemental Material [24] including comparison the blowout bubbles driven by Gaussian and flat-top beams, respectively [31].

The authors would like to thank Nathan Majernik for insightful discussions. This work was performed with the support of the US Dept. of Energy under Contract No. DE-SC0017648 and DE0SC0009914. This work used resources of the National Energy Research Scientific Computing Center, a US DOE Office of Science User Facility, operated under Contract No. DE-AC02-05CH11231.

APPENDIX

We start with the analysis done by Regenstreif to find the potential and field produced by a uniform beam with charge density ρ inside a confocal vacuum chamber[32]. We define two boundaries: one for the vacuum chamber and one for the beam, respectively $\mu = \mu_1$ and $\mu = \mu_0$.

$$\begin{aligned} \psi_{\mu > \mu_0} &= \frac{\rho c_p^2}{8} \left[2(\mu_1 - \mu) - \frac{\sinh 2(\mu_1 - \mu)}{\cosh 2\mu_1} \cos 2\nu \right] \sinh 2\mu_0 \\ \psi_{\mu < \mu_0} &= \frac{\rho c_p^2}{8} \left(\left[\frac{\cosh 2(\mu_1 - \mu_0)}{\cosh 2\mu_1} \cosh 2\mu - 1 \right] \cos 2\nu \right. \\ &\quad \left. + \cosh 2\mu_0 - \cosh 2\mu + 2(\mu_1 - \mu_0) \sinh 2\mu_0 \right) \end{aligned} \quad (\text{A1})$$

Taking the chamber to be at infinity, $\mu_1 \rightarrow \infty$, we have the substitutions $\lim_{\mu_1 \rightarrow \infty} \frac{\sinh(2\mu_1 - 2\mu)}{\cosh 2\mu_1} = \cosh 2\mu - \sinh 2\mu$ and $\lim_{\mu_1 \rightarrow \infty} \frac{\cosh(2\mu_1 - 2\mu_0)}{\cosh 2\mu_1} = \cosh 2\mu_0 - \sinh 2\mu_0$. Ignoring the constant term that contributes to infinity, a solution for the isolated beam can be obtained:

$$\begin{aligned} \psi_{\mu > \mu_0} &= -\frac{\rho c_p^2}{8} [2\mu + (\cosh 2\mu - \sinh 2\mu) \cos 2\nu] \sinh 2\mu_0 \\ \psi_{\mu < \mu_0} &= -\frac{\rho c_p^2}{8} \left([1 - (\cosh 2\mu_0 - \sinh 2\mu_0) \cosh 2\mu] \cos 2\nu \right. \\ &\quad \left. + \cosh 2\mu_0 - \cosh 2\mu - 2\mu_0 \sinh 2\mu_0 \right) \end{aligned} \quad (\text{A2})$$

We can use this analysis, to construct the source term, $S = \rho - J_z$ by using two confocal ellipses overlapping each other; $\mu_{in} = \mu_0$ and $\mu_{out} = \mu_0 + \Delta_s$. To yield the desired source distribution defined in the paper, we set the source densities to be $S_{in} = -S_{\Delta_s}$ and $S_{out} = \rho_i + S_{\Delta_s}$. Applying the conservation of S in the transverse plane, $\int_0^{2\pi} \int_0^{\mu_{out}} (S_{in} + S_{out}) \frac{c_p^2}{2} (\cosh 2\mu - \cos 2\nu) d\mu d\nu = 0$, yielding:

$$S_{\Delta_s} = -\frac{\rho_i \sinh(\mu_0 + \Delta_s)}{\sinh(\mu_0 + \Delta_s) - \sinh \mu_0} \quad (\text{A3})$$

We now have the complete form of the source density and can find the ψ using the superposition of the wake potentials of the two confocal ellipses. The combination of the conservation of the source term and the confocal-ity condition has a key property: outside the sheath, the wakefield due to the sheath cancels out the wakefield due to the ion column, i.e $\psi|_{\mu > \mu_0} = 0$. The confocal model works well to capture this essential quality of the blowout regime, showing the elliptical symmetry of the fields. We are also interested in the form of ψ inside the ion column

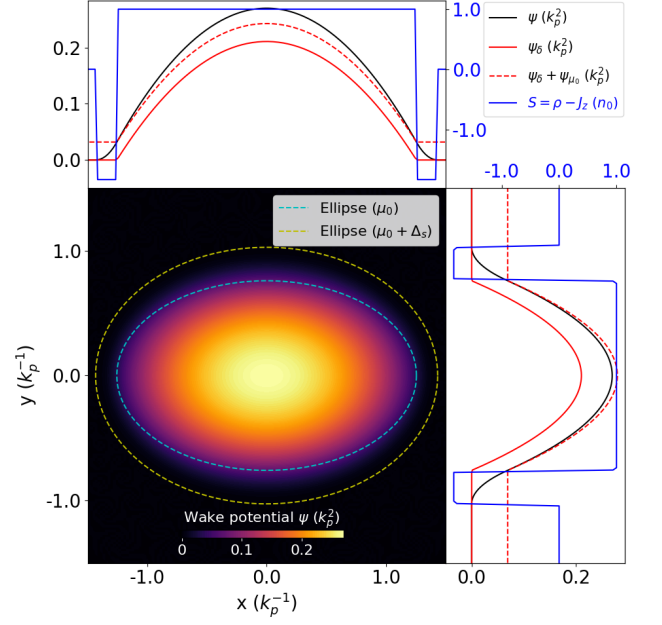


FIG. A1: Wake potential calculated for a specific set of parameters ($c_p = 1$, $\mu_0 = 0.7$, $\Delta_s = 0.2$). The plot illustrates the shape of the wake potential ψ with the corresponding line-outs along the x and y axes. It also includes the line-outs of the source term S and the delta-function potential ψ_δ .

to calculate the wakefields, and inside the sheath to calculate the electron trajectories. This can be calculated from the isolated beam solutions.

Here, we simplify the former by introducing the assumption that the sheath thickness is small compared to the ion column ($\Delta_s/\mu_0 < 1$), yielding the solutions (up to first order in Δ_s):

$$\begin{aligned} \psi|_{\mu < \mu_0} &= -\frac{c_p^2}{8} \left[\cosh 2\mu - \cosh 2\mu_0 + \left(1 - \frac{\cosh 2\mu}{\cosh 2\mu_0} \right) \cos 2\nu \right. \\ &\quad \left. + \Delta_s \left(\sinh 2\mu_0 - \tanh 2\mu_0 \frac{\cosh 2\mu}{\cosh 2\mu_0} \cos 2\nu \right) \right] \end{aligned} \quad (\text{A4})$$

If we assume the sheath to be infinitesimal ($\Delta_s \rightarrow 0$), there is an alternative method that can be used to arrive at the same solution. Assuming no electromagnetic fields exist outside the blowout due to the shielding provided by the sheath at $\partial\Omega(\xi)$, we may then set the wake potential to be zero everywhere outside the blowout region. Finally, the constant charge density inside the cavity from the ions alone enables us to solve for the wake. In this case, we have: $\nabla_\perp^2 \psi_\delta(\xi) = -1$, with $\psi_\delta|_{\partial\Omega(\xi)} = 0$. In this

case, the particular solution is:

$$\psi_{\delta,p} = -\frac{a^2}{8} (\cosh(2\mu) - \cosh(2\mu_0) + \cos(2v)) \quad (\text{A5})$$

We add a homogeneous solution such that potential is 0 at $\mu = \mu_0$:

$$\psi_{\delta,h} = \frac{a^2}{8} \left(\frac{\cosh(2\mu)}{\cosh(2\mu_0)} \right) \cos(2v) \quad (\text{A6})$$

Adding the particular and homogenous solutions gives us the same result as $\lim_{\Delta_s \rightarrow 0} \psi = \psi_\delta$.

$$\psi_\delta = -\frac{c_p^2}{8} \left(\cosh 2\mu - \cosh 2\mu_0 + \left(1 - \frac{\cosh 2\mu}{\cosh 2\mu_0} \right) \cos 2\nu \right) \quad (\text{A7})$$

The exact wake potential solution including the sheath, along with the solution from the delta function approximation is shown in Fig. A1. Adding an offset to the delta function approximation allows us to study the differences between the two wake potential profiles. This comparison is crucial for analyzing the gradients wakefields), which are of primary interest.

* pkmanwani@gmail.com

- [1] P. Chen, Differential luminosity under multiphoton beamstrahlung, *Phys. Rev. D* **46**, 1186 (1992).
- [2] S. Lee, T. Katsouleas, P. Muggli, W. B. Mori, C. Joshi, R. Hemker, E. S. Dodd, C. E. Clayton, K. A. Marsh, B. Blue, S. Wang, R. Assmann, F. J. Decker, M. Hogan, R. Iverson, and D. Walz, Energy doubler for a linear collider, *Phys. Rev. ST Accel. Beams* **5**, 011001 (2002).
- [3] P. Chen, J. M. Dawson, R. W. Huff, and T. Katsouleas, Acceleration of electrons by the interaction of a bunched electron beam with a plasma, *Phys. Rev. Lett.* **54**, 693 (1985).
- [4] J. B. Rosenzweig, B. Breizman, T. Katsouleas, and J. J. Su, Acceleration and focusing of electrons in two-dimensional nonlinear plasma wake fields, *Phys. Rev. A* **44**, R6189 (1991).
- [5] N. Barov, J. B. Rosenzweig, M. E. Conde, W. Gai, and J. G. Power, Observation of plasma wakefield acceleration in the underdense regime, *Phys. Rev. ST Accel. Beams* **3**, 011301 (2000).
- [6] W. Lu, C. Huang, M. Zhou, W. B. Mori, and T. Katsouleas, Nonlinear theory for relativistic plasma wakefields in the blowout regime, *Phys. Rev. Lett.* **96**, 165002 (2006).
- [7] S. A. Yi, V. Khudik, C. Siemon, and G. Shvets, Analytic model of electromagnetic fields around a plasma bubble in the blow-out regime, *Physics of Plasmas* **20**, 013108 (2013), https://pubs.aip.org/aip/pop/article-pdf/doi/10.1063/1.4775774/13429408/013108_1.online.pdf.
- [8] N. Barov, J. B. Rosenzweig, M. C. Thompson, and R. B. Yoder, Energy loss of a high-charge bunched electron beam in plasma: Analysis, *Phys. Rev. ST Accel. Beams* **7**, 061301 (2004).
- [9] J. B. Rosenzweig, N. Barov, M. C. Thompson, and R. B. Yoder, Energy loss of a high charge bunched electron beam in plasma: Simulations, scaling, and accelerating wakefields, *Phys. Rev. ST Accel. Beams* **7**, 061302 (2004).
- [10] S. S. Baturin, Flat bubble regime and laminar plasma flow in a plasma wakefield accelerator, *Phys. Rev. Accel. Beams* **25**, 081301 (2022).
- [11] P. Manwani *et al.*, Beam Matching in an Elliptical Plasma Blowout Driven by Highly Asymmetric Flat Beams, in *Proc. IPAC'22*, International Particle Accelerator Conference No. 13 (JACoW Publishing, Geneva, Switzerland, 2022) pp. 1802–1805.
- [12] P. Manwani, N. Majernik, J. Mann, Y. Kang, D. Chow, H. Ancelin, G. Andonian, and J. Rosenzweig, Flat beam plasma wakefield accelerator (2023), arXiv:2305.01902 [physics.acc-ph].
- [13] T. Raubenheimer, An afterburner at the ilc: The collider viewpoint 10.2172/833030 (2004).
- [14] R. A. Fonseca, S. F. Martins, L. O. Silva, J. W. Tonge, F. S. Tsung, and W. B. Mori, One-to-one direct modeling of experiments and astrophysical scenarios: pushing the envelope on kinetic plasma simulations, *Plasma Physics and Controlled Fusion* **50**, 124034 (2008).
- [15] J. M. Dawson, Nonlinear electron oscillations in a cold plasma, *Phys. Rev.* **113**, 383 (1959).
- [16] J. B. Rosenzweig, A. M. Cook, A. Scott, M. C. Thompson, and R. B. Yoder, Effects of ion motion in intense beam-driven plasma wakefield accelerators, *Phys. Rev. Lett.* **95**, 195002 (2005).
- [17] P. Sprangle, E. Esarey, and A. Ting, Nonlinear interaction of intense laser pulses in plasmas, *Phys. Rev. A* **41**, 4463 (1990).
- [18] P. Mora and T. M. Antonsen, Jr., Kinetic modeling of intense, short laser pulses propagating in tenuous plasmas, *Physics of Plasmas* **4**, 217 (1997), https://pubs.aip.org/aip/pop/article-pdf/4/1/217/12532941/217_1.online.pdf.
- [19] W. Lu, C. Huang, M. Zhou, M. Tzoufras, F. S. Tsung, W. B. Mori, and T. Katsouleas, A nonlinear theory for multidimensional relativistic plasma wave wakefields), *Physics of Plasmas* **13**, 056709 (2006), https://pubs.aip.org/aip/pop/article-pdf/doi/10.1063/1.2203364/15804477/056709_1.online.pdf.
- [20] A. Golovanov, I. Y. Kostyukov, A. Pukhov, and V. Malka, Energy-conserving theory of the blowout regime of plasma wakefield, *Phys. Rev. Lett.* **130**, 105001 (2023).
- [21] W. K. H. Panofsky and W. A. Wenzel, Some Considerations Concerning the Transverse Deflection of Charged Particles in Radio-Frequency Fields, *Review of Scientific Instruments* **27**, 967 (1956), https://pubs.aip.org/aip/rsi/article-pdf/27/11/967/19098135/967_1.online.pdf.
- [22] M. R. Shubaly, Space charge fields of elliptically symmetrical beams, *Nuclear Instruments and Methods* **130**, 19 (1975).
- [23] G. Parzen, Electric fields of a uniformly charged elliptical beam (2001), arXiv:physics/0108040 [physics.acc-ph].
- [24] See supplemental material at [url will be inserted by publisher] for details on pic simulations and computational methods.
- [25] P. Manwani, A. Ody, D. Chow, G. Andonian, J. Rosenzweig, and Y. Kang, Flat beam transport for a PWFA experiment at AWA, in *Proc. IPAC'24*, International Par-

- ticle Accelerator Conference No. 15 (JACoW Publishing, Geneva, Switzerland, 2024) pp. 580–582.
- [26] T. Tajima and J. M. Dawson, Laser electron accelerator, *Phys. Rev. Lett.* **43**, 267 (1979).
 - [27] T. Xu, M. Conde, G. Ha, M. Kuriki, P. Piot, J. Power, and E. Wisniewski, Generation High-Charge of Flat Beams at the Argonne Wakefield Accelerator, in *10th International Particle Accelerator Conference* (2019).
 - [28] P. Manwani *et al.*, Asymmetric Beam Driven Plasma Wakefields at the AWA, in *Proc. IPAC'21* (JACoW Publishing, Geneva, Switzerland) pp. 1732–1735.
 - [29] M. Yadav *et al.*, Radiation Diagnostics for AWA and FACET-II Flat Beams in Plasma, in *Proc. IPAC'22*, International Particle Accelerator Conference No. 13 (JACoW Publishing, Geneva, Switzerland, 2022) pp. 1791–1794.
 - [30] Manwani *et al.*, Propagation of beams inside a transversely elliptical blowout plasma wakefield (2024), manuscript in preparation.
 - [31] Y. K. et al., Comparison of flat beam pwfa analytic model with pic simulations, in *Proc. IPAC'24*, IPAC'24 - 15th International Particle Accelerator Conference No. 15 (JACoW Publishing, Geneva, Switzerland, 2024) pp. 583–586.
 - [32] E. Regenstreif, Potential and field produced by a uniform or non-uniform elliptical beam inside a confocal elliptic vacuum chamber, *IEEE Trans. Nucl. Sci.*; (United States) (1977).